Eur. Phys. J. A (2017) **53**: 88
DOI 10.1140/epja/i2017-12268-7

THE EUROPEAN PHYSICAL JOURNAL A

Regular Article – Theoretical Physics

Asymmetry dependence of Gogny-based optical potential*

G. Blanchon[1,a], M. Dupuis[1], R.N. Bernard[1], and H.F. Arellano[2,1]

[1] CEA, DAM, DIF F-91297 Arpajon, France
[2] Department of Physics - FCFM, University of Chile, Av. Blanco Encalada 2008, Santiago, Chile

Received: 1 December 2016 / Revised: 7 March 2017
Published online: 11 May 2017 – © Società Italiana di Fisica / Springer-Verlag 2017
Communicated by N. Alamanos

Abstract. An analysis of neutron and proton scattering off ^{40,48}Ca has been carried out. Real and imaginary potentials have been generated using the Nuclear Structure Method (NSM) for scattering with the Gogny D1S nucleon-nucleon effective interaction. Observables are well described by NSM for neutron and proton elastic scattering off ^{40}Ca and for neutron scattering off ^{48}Ca. For proton scattering off ^{48}Ca, NSM yields a lack of absorption. This discrepancy is attributed to two-fold charge exchange (p, n, p) contribution and coupling to Gamow-Teller mode which are not included in the present version of NSM. A recipe based on a Perey-Buck fit of the NSM imaginary potential and Lane model is proposed to overcome this issue in an approximate way.

1 Introduction

Optical potentials are key for the description of nucleon-nucleus direct elastic and inelastic scatterings [1]. Moreover, they are used to generate transmission coefficients for the statistical model of a compound nucleus such as in the Hauser-Feshbach formalism [2] and beyond [3,4]. Furthermore, the knowledge of the isospin asymmetry dependence of the potential is convenient when calculating quasielastic charge-exchange processes. For evaluation purposes, optical potentials are often fitted in order to reproduce a consistent set of reaction observables. Whenever experimental data are not available, one can ideally rely on more microscopic approaches such as Nuclear Field Theory [5,6], Energy Density Functionals (EDF) [7–10], *ab initio* approaches [11,12] or mixed approaches such as g-matrix effective interaction folded with EDF density [13,14]. Moreover microscopic approaches can be used to guide new parametrizations of phenomenological potentials, providing form factors for volume and surface parts of the potential, energy dependence, nonlocality shape and parameters, as well as dependence on the isospin asymmetry of the target nucleus.

In previous attempts [9,15], the Nuclear Structure Method [7] has been successfully applied to describe nucleon scattering off ^{40}Ca using Gogny D1S interaction as sole input. This method is based on Green's function formalism. In its current version, it allows the description of nucleon scattering off doubly-closed-shell spherical nuclei including integral and differential cross sections as well as spin observables below about 30 MeV incident energy. An extension to target nuclei with pairing and deformed target nuclei will be possible in a near future thanks to EDF extended reach. It is worth noting that Gogny interaction has been originally fitted on structure observables. The nice agreement with reaction observables provided by NSM is mainly due to the correct description of the target-nucleus radius and the good description of collective excited states of the target nucleus provided by the Random-Phase Approximation (RPA) for doubly-closed shell nuclei.

In this work, we apply NSM to nucleon scattering off both ^{40}Ca and ^{48}Ca in order to study optical potential dependence on the isospin asymmetry of the target nucleus. In sect. 2, we present a brief reminder of the NSM formalism. In sect. 3, in order to assess the validity of the NSM potential, we confront NSM reaction observables with data. In sect. 4, volume integrals for NSM imaginary potential are presented with a special focus on the isospin asymmetry of the target. In sect. 5, general trends of the NSM potential are extracted by fitting a Perey-Buck-like equivalent potential [16]. Then an approximation based on Lane consistency [17] is used in order to recover the missing absorption in the case of proton scattering off ^{48}Ca. Finally, in sect. 6 we present the main conclusions of this study.

* Contribution to the Topical Issue "Finite range effective interactions and associated many-body methods - A tribute to Daniel Gogny" edited by Nicolas Alamanos, Marc Dupuis, Nathalie Pillet.

[a] e-mail: guillaume.blanchon@cea.fr

2 Nuclear Structure Method

The NSM formalism has already been presented in some detail in refs. [9,15]. We briefly introduce here the key points of the formalism. Equations are presented omitting spin for simplicity. The NSM potential, V, consists of two components:

$$V = V^{HF} + \Delta V. \tag{1}$$

The former is a mean-field potential; the latter is a polarization potential built from target-nucleus excitations. The explicit coupling of the elastic channel to those inelastic channels results in a loss of flux which is reflected in the imaginary part of the complex ΔV potential.

The Hartree-Fock (HF) potential in coordinate space reads

$$V^{HF}(\mathbf{r},\mathbf{r}') = \int \mathrm{d}\mathbf{r}_1 v(\mathbf{r},\mathbf{r}_1)\rho(\mathbf{r}_1)\delta(\mathbf{r}-\mathbf{r}') - v(\mathbf{r},\mathbf{r}')\rho(\mathbf{r},\mathbf{r}'), \tag{2}$$

where v is the effective NN interaction. $\rho(\mathbf{r})$ and $\rho(\mathbf{r},\mathbf{r}')$ are the usual local and nonlocal densities [9], respectively. Rearrangement contributions stemming from the density-dependent term of the interaction are also accounted for [18].

The polarization potential, ΔV in eq. (1), is built by coupling the elastic channel to the intermediate excited states of the target nucleus. These excited states are described within the RPA formalism [18]. Both excited states and couplings are generated using the same NN effective interaction. The resulting potential is nonlocal, energy dependent and complex. Going into more details, the polarization contribution to the potential reads

$$\Delta V = V^{PP} + V^{RPA} - 2V^{(2)}, \tag{3}$$

where V^{PP} and V^{RPA} are contributions from particle-particle and particle-hole correlations, respectively. The uncorrelated particle-hole contribution, $V^{(2)}$, is accounted for once in V^{PP} and twice in V^{RPA}. It is subtracted twice in order to avoid double counting. When using Gogny interaction, part of particle-particle correlations is already contained at the HF level. We use the same prescription as in ref. [19], omitting the real part of V^{PP} while approximating the imaginary part of V^{PP} by $\mathrm{Im}[V^{(2)}]$. The resulting potential is not fully dispersive anymore due to this last term, which does not have any real counterpart. Then eq. (3) reduces to

$$\Delta V = \mathrm{Im}\left[V^{(2)}\right] + V^{RPA} - 2V^{(2)}. \tag{4}$$

For nucleons with incident energy E, the RPA potential reads,

$$V^{RPA}(\mathbf{r},\mathbf{r}',E) = \sum_{N\neq 0} \sum\!\!\!\!\!\!\int_{\lambda} \left[\frac{n_\lambda}{E-\varepsilon_\lambda+E_N-i\Gamma(E_N)} + \frac{1-n_\lambda}{E-\varepsilon_\lambda-E_N+i\Gamma(E_N)}\right] \times \Omega^N_\lambda(\mathbf{r})\Omega^N_\lambda(\mathbf{r}'), \tag{5}$$

where n_i and ε_i are occupation number and energy of the single-particle state ϕ_i in the HF field, respectively. The label λ refers to the single-particle state of the intermediate particle [15]. E_N and $\Gamma(E_N)$ represent the energy and the width of the N-th excited state of the target, respectively. Additionally,

$$\Omega^N_\lambda(\mathbf{r}) = \sum_{(p,h)} \left[X^{N,(p,h)}F_{ph\lambda}(\mathbf{r}) + Y^{N,(p,h)}F_{hp\lambda}(\mathbf{r})\right], \tag{6}$$

where X and Y denote the usual RPA amplitudes and

$$F_{ij\lambda}(\mathbf{r}) = \int \mathrm{d}^3\mathbf{r}_1 \phi^*_i(\mathbf{r}_1) v(\mathbf{r},\mathbf{r}_1)\left[1-\hat{\mathrm{P}}\right]\phi_\lambda(\mathbf{r})\phi_j(\mathbf{r}_1), \tag{7}$$

where $\hat{\mathrm{P}}$ is a particle-exchange operator and v is the same effective NN interaction as in eq. (2). The uncorrelated particle-hole contribution reads

$$V^{(2)}(\mathbf{r},\mathbf{r}',E) = \frac{1}{2}\sum_{ij}\sum\!\!\!\!\!\!\int_{\lambda} \left[\frac{n_i(1-n_j)n_\lambda}{E-\varepsilon_\lambda+E_{ij}-i\Gamma(E_{ij})} + \frac{n_j(1-n_i)(1-n_\lambda)}{E-\varepsilon_\lambda-E_{ij}+i\Gamma(E_{ij})}\right] \times F_{ij\lambda}(\mathbf{r})F^*_{ij\lambda}(\mathbf{r}'), \tag{8}$$

with $E_{ij} = \varepsilon_i - \varepsilon_j$, the uncorrelated particle-hole energy.

Calculations are performed according to the following scheme:

- The nonlocal HF potential, V^{HF} in eq. (2), is calculated self-consistently using Gogny D1S interaction [20]. This is done in coordinate space by diagonalization in a 15 fm box to ensure the correct asymptotic behavior of single-particle states.
- V^{HF} is used as well to generate the intermediate single-particle state labeled λ in eqs. (5) and (8). Both discrete and continuum spectra of the intermediate single-particle state are accounted for. The continuum single-particle spectrum is generated neither localizing HF potential nor discretizing in a box. The integro-differential Schrödinger equation for scattering with the nonlocal potential is solved following the matrix inversion method exposed in the documentation of the DWBA code [21] connecting to corresponding asymptotic solution. This method allows to take into account the resonances in the intermediate single-particle states known to have a striking effect on absorption [15,22].
- Target excited states are obtained solving RPA equations in a harmonic-oscillator basis, including fifteen major shells [23] and using Gogny D1S interaction. We account for all the RPA excited states with spin up to $J = 8$. The use of a harmonic-oscillator basis discretizes the excitations of the target nucleus which results in nonorthogonality between the intermediate λ state and the RPA excitations. Nevertheless, these effects are small. One should ideally use continuum-RPA [24] as starting point for the description of excitations.

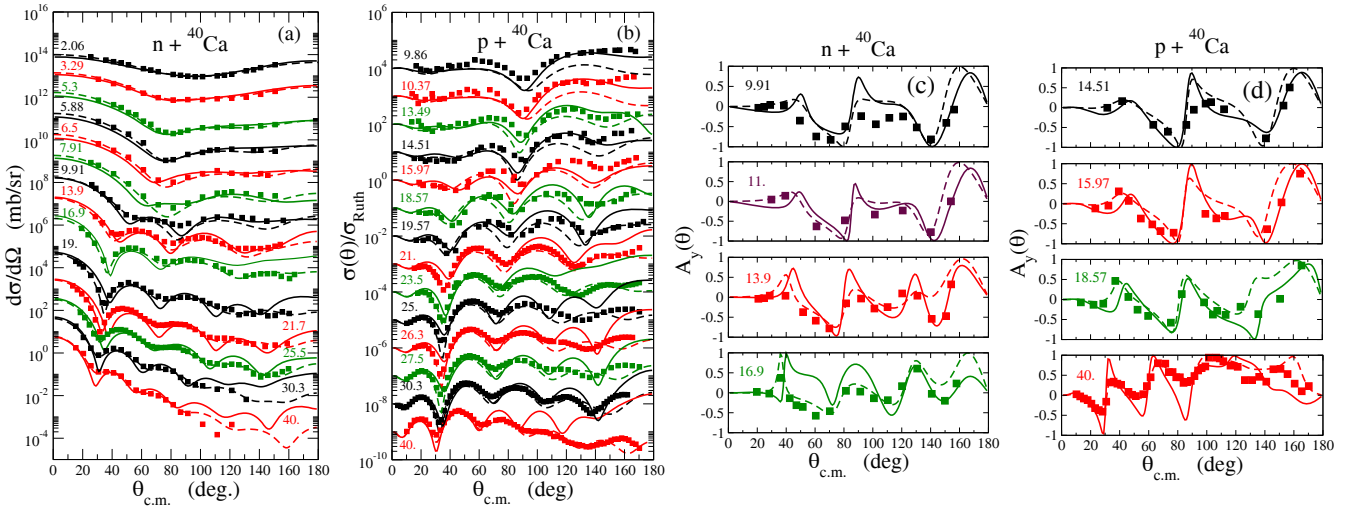

Fig. 1. Differential cross sections for neutron (a) and proton (b) scattering off ^{40}Ca. Comparison between data (symbols), $V^{HF} + \Delta V$ results (solid curves) and Koning-Delaroche potential results (dashed curves). The same for analyzing powers for neutron (c) and proton (d) scattering. Incident energies are indicated in MeV.

- V^{RPA} and $V^{(2)}$ are obtained using Gogny D1S interaction in eqs. (5).
- The first zero-energy $J^\pi = 1^-$ excited state obtained with RPA, containing the spurious translational mode, is removed from the calculation in eqs. (5).
- Escape and damping widths are simulated assigning a single phenomenological width, $\Gamma(E_N)$, to RPA states and uncorrelated particle-hole excitations in eqs. (5) and (8). $\Gamma(E_N)$ takes the value of 2, 5, 15 and 50 MeV, for excitation energies of 20, 50, 100 and 200 MeV, respectively. For incident energies above about 10 MeV, where the compound elastic contribution is negligible, cross sections are not very sensitive to the value chosen for the width [15].
- Two-fold charge exchanges (p, n, p) and (n, p, n) are not accounted for in the present version of NSM, thus the intermediate single-particle state λ is of the same isospin projection than the incident and the outgoing particle.

The HF propagator is dressed only once. For this reason the scheme is self-consistent at the HF level and only consistent when considering polarization contributions.

3 Microscopic potential and reaction data

Before going further into the analysis of the NSM potential, we first check its ability to reproduce experimental reaction observables. NSM has been applied to neutron and proton scattering off ^{40,48}Ca using Gogny D1S interaction. We focus on incident energies below 40 MeV where NSM has demonstrated to be promising in the case of ^{40}Ca target [9,15]. Results are summarized in figs. 1 and 2. References to data are given in ref. [25]. Compound-elastic corrections furnished by the Hauser-Feshbach formalism [2] using the Koning-Delaroche potential [25] with TALYS [26] are applied to cross sections obtained from NSM and Koning-Delaroche potentials. This correction results in an improved description of cross sections for neutron scattering with incident energy below 10 MeV.

In the case of neutron scattering off ^{40,48}Ca (figs. 1(a) and 2(a), respectively), NSM results reasonably agree with experiment and results based on the Koning-Delaroche potential up to about 30 MeV incident energy. Even if not perfect, those results are encouraging considering the fact that Gogny interaction was not initially designed for scattering purposes. Still, there is room for improvements for example forging new NN effective interactions including scattering observables in the fit procedure as done in ref. [27]. Regarding proton scattering, NSM yields fair results for ^{40}Ca target up to 30 MeV incident proton energy (fig. 1(b)) but demonstrates an important lack of absorption at all incident energies in the case of ^{48}Ca target (fig. 2(b)), nevertheless, the correct shape of the differential cross section is retained. In figs. 1(c) and 1(d), we show the calculated analyzing powers for neutron and proton scattering off ^{40}Ca, at several incident energies, in good agreement with experiment. In fig. 2(d), analyzing powers for proton scattering off ^{48}Ca compare quite well with experiments. Moreover, agreement with data is comparable to that obtained from the Koning-Delaroche potential. These results suggest that NSM potential retains the correct spin-orbit behavior even in the case of proton-neutron asymmetry in the target nucleus. To our knowledge, analyzing powers for neutron scattering off ^{48}Ca are not available experimentally in this energy range. In fig. 2(c), we present analyzing power predictions between 4.7 MeV and 16.8 MeV incident neutron energy. NSM description shows slight differences with Koning-Delaroche predictions.

In fig. 3(a), total cross sections for neutron scattering from both ^{40,48}Ca targets are in good agreement with ex-

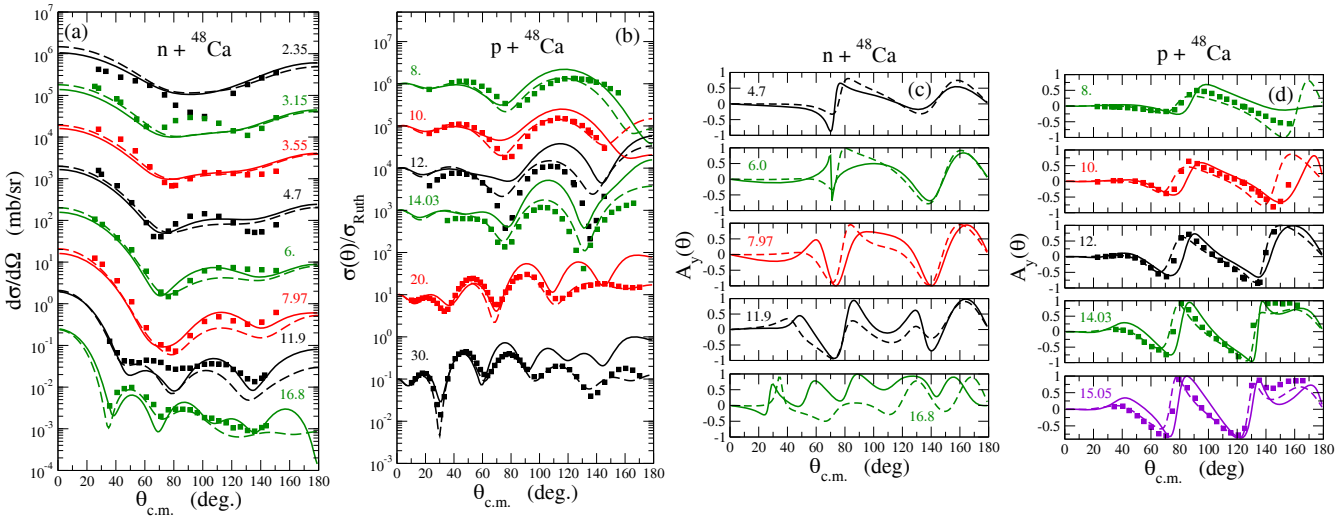

Fig. 2. Same as fig. 1 for ^{48}Ca.

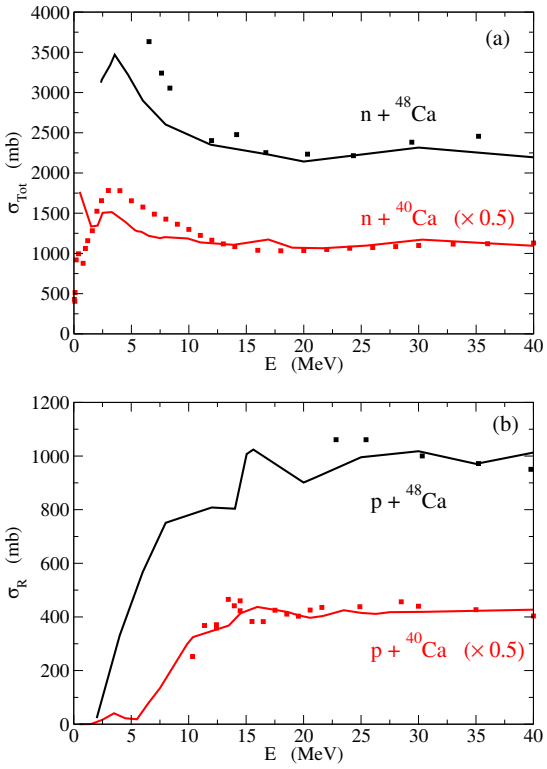

Fig. 3. Total cross section for neutron scattering off ^{40,48}Ca (a). Reaction cross section for proton scattering off ^{40,48}Ca (b).

periment above about 10 MeV incident energy. Below that energy, total cross sections are underestimated by NSM. In fig. 3(b), we show reaction cross sections for proton scattering from both ^{40,48}Ca targets. NSM results are in good agreement with experiment. In the case of ^{48}Ca, fewer experimental measurements are available between 22 MeV and 40 MeV.

We wish now to investigate what makes NSM up to describe neutron and proton scattering off ^{40}Ca and what makes it fail in reproducing proton scattering off ^{48}Ca.

Charity *et al.* have investigated extensively the asymmetry dependence of dispersive optical potentials in calcium isotopes [28–30]. They reached the conclusion that for proton elastic scattering, an increase in the absorption is expected in going from ^{40}Ca to ^{48}Ca because of the coupling to the Gamow-Teller collective mode [29]. It is argued that this could enhance surface absorption with strength increasing as $\sim 3(N-Z)$. On the other hand, no change is expected for neutrons, as they do not couple to this resonance. In a further attempt, Waldecker *et al.* [31] studied asymmetry from an *ab-initio* point of view using Faddeev Random-Phase Approximation (FRPA) [32]. Results suggest that charge-exchange excitations of the target interfere only very weakly with the nucleon-nucleus scattering process. The most striking effect on the potential related to isospin asymmetry is related to the tensor term of the bare interaction which plays a major role on absorption in FRPA.

What does NSM contain? In NSM, the $(A+1)$-body system consisting of an incident nucleon and A target nucleons, is described as a single-particle state in the HF field labeled λ in eq. (5) and an RPA state describing target excitations at the one particle - one hole level. This description of the $(A+1)$-body system allows to span only partially over the $(A+1)$-nucleon Hilbert space. As a result, at this level of approximation, NSM deals with processes involving 0, 1 and 2 nucleons in the continuum, depending on whether the single-particle state is bound and the RPA excitation involves bound particle states; the single-particle state is in the continuum or the RPA excitation involves continuum particle states; and both are in the continuum, respectively. Thus, NSM gives access to part of the direct emission of proton, neutron, neutron-

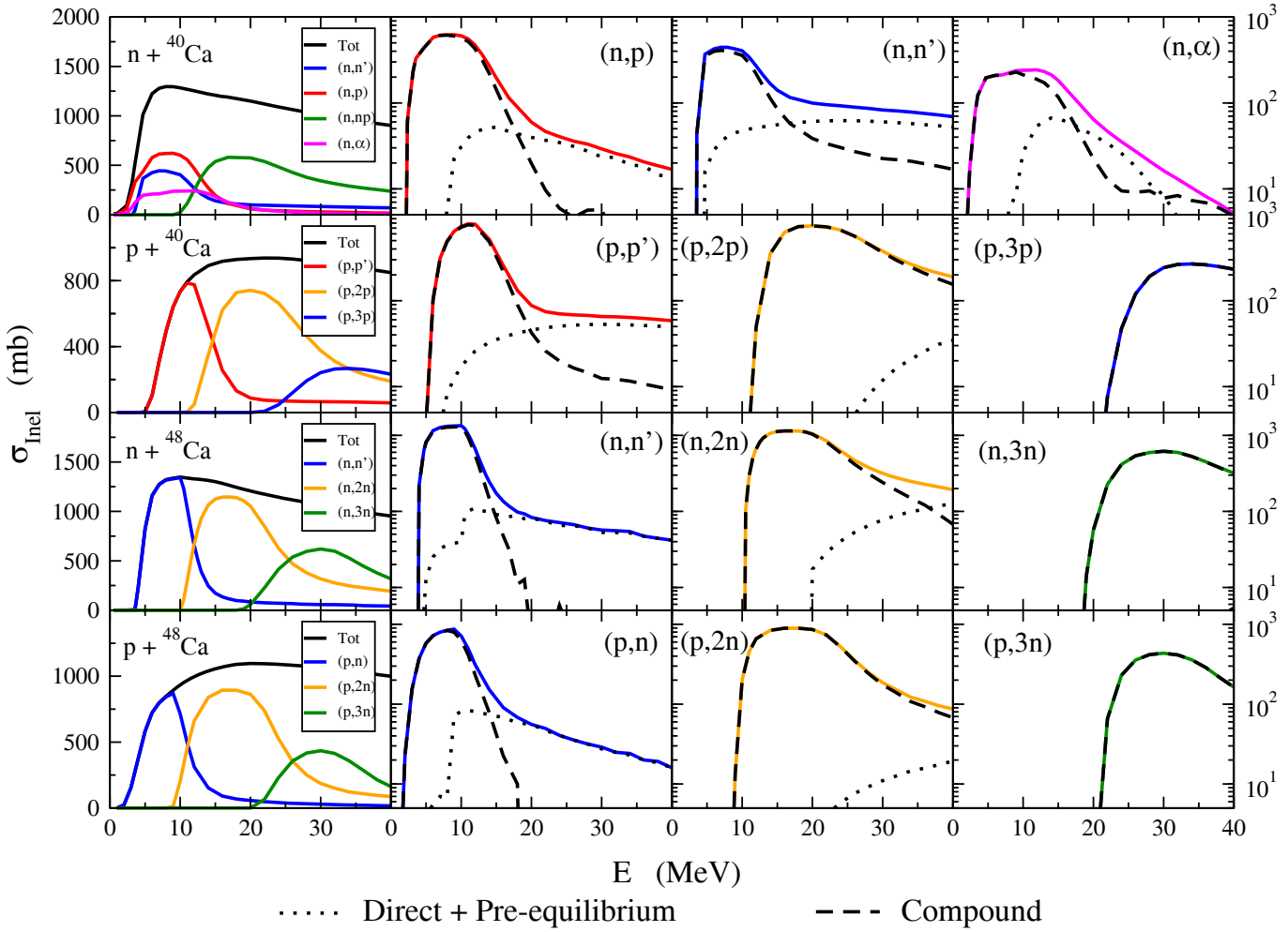

Fig. 4. (Color online) TALYS evaluations of inelastic cross sections for neutron and proton scattering off ^{40,48}Ca: Total reaction cross section (with linear scale on the left-hand side) and the main components responsible for absorption (with logarithmic scale on the right-hand side). Direct and Pre-equilibrium inelastic contributions are summed and are depicted in dotted line. Compound inelastic contributions are in dashed line.

proton pair and deuteron. Once again, the use of a continuum RPA [24] instead of an RPA projected on harmonic-oscillator basis [23] would certainly improve the description of these processes. Moreover, in its present version, NSM does not explicitly account for two-fold charge exchanges (n, p, n) and (p, n, p), meaning that the λ intermediate single-particle state has the same isospin projection than the incident particle. This inhibits coupling to the Gamow-Teller collective mode as well as proton (neutron) pair direct emission in the case of neutron (proton) scattering. Moreover, heavier composite particles such as tritium and α particles or more generally the direct emission of more than two nucleons would require a description of the target nucleus with higher order in perturbation, such as second RPA [33] or multiparticle-multihole configuration mixing [34]. A direct reaction is a doorway leading toward compound nucleus formation. The compound nucleus is formed by a sequence of collisions, namely the pre-equilibrium, leading to increasingly complicated rearrangements of the target nucleus. NSM describes only the first step of this sequence taking into account $2p-1h$ excitations with coherent particle-hole amplitudes provided by RPA. The phenomenological width applied to RPA states makes possible the damping toward compound nucleus.

NSM vs. evaluation. Bearing the above considerations in mind, we study neutron and proton scattering off ^{40,48}Ca targets below 40 MeV with the nuclear reaction code TALYS [26]. This evaluation tool deals with numerous reaction channels including direct, pre-equilibrium and compound reaction mechanisms. In particular, it provides a quantitative picture of the various particles emitted during the scattering process. The direct contribution is obtained through the coupling to experimentally known collective states. The corresponding coupled-channel problem is solved with ECIS code [35]. The pre-equilibrium is obtained with the exciton model where target excitations are described within a particle-hole scheme. For in-

cident energies below about 40 MeV, after primary pre-equilibrium emission, the excitation energy of the residual nucleus is relatively small and one can safely assume that further decay of the nucleus proceeds mainly by compound mechanism [36]. The multiple pre-equilibrium emission is very weak. In fig. 4, we present the corresponding inelastic cross sections together with the main contributions to absorption. The distinction between the direct part and the pre-equilibrium mechanisms is rather arbitrary, especially under 20 MeV, so we present the sum of the two contributions. In the following we shall refer to it as direct contribution.

For ^{40,48}Ca targets within the energy range considered, TALYS results suggest that deuteron direct emission is negligible. As a result, the explicit coupling to intermediate deuteron is not relevant in this study.

In the case of neutron scattering off ^{48}Ca, the main components of the absorption ordered by increasing threshold energy are (n, n'), $(n, 2n)$ and $(n, 3n)$. The (n, n') component is led by compound emission below about 15 MeV and by direct emission above. The following neutron multi-emission components are mostly of compound nature. Good results obtained with NSM are explained by the fact that (n, n') is taken into account explicitly and it is the main doorway state.

The same logic holds for proton scattering off ^{40}Ca where the main components of absorption are (p, p'), $(p, 2p)$ and $(p, 3p)$. The direct (p, p') contribution is described within NSM and acts as a doorway that feeds the compound $(p, 2p)$ and $(p, 3p)$ contributions.

For neutron scattering off ^{40}Ca, the main components are (n, p), (n, n') and (n, np). The (n, np) contribution, not depicted in fig. 4, is mainly compound. The important contribution from (n, p) is due to a low threshold energy for this reaction channel, about 500 keV, compared to the case of (n, n'), of about 3.5 MeV. These last two components are partly contained in NSM, where (n, n') is explicitly taken into account and (n, p) is partly accounted for with proton RPA excitations in the continuum. The inclusion of two-fold charge exchange in the formalism would improve NSM prediction in that case. Moreover, at low energy TALYS code yields an (n, α) component with some direct contribution. The coupling to the α intermediate channel is beyond the scope of this work. Still, results obtained with NSM for neutron scattering off ^{40}Ca are reasonable.

In the case of proton scattering off ^{48}Ca, the absorption is mainly built from (p, n), $(p, 2n)$ and $(p, 3n)$ channels. The last two contributions are mainly compound while the (p, n) channel has a direct component expected to be described only partially by NSM with neutron excitations in the continuum described with RPA. Most part of (p, n) channel may be obtained from two-fold charge exchange. Once again, this contribution is not accounted for by NSM, which could explain the lack of absorption observed in differential elastic cross section for proton scattering off ^{48}Ca in fig. 2(b).

To conclude this part, there are strong indications that coupling to Gamow-Teller mode would improve the NSM description of proton scattering off ^{48}Ca. More generally, coupling to Gamow-Teller mode should play an important role when dealing with proton scattering off neutron-rich targets close to the neutron drip-line as neutron emission is favored.

NSM & tensor interaction. Waldecker *et al.* pointed out the major influence of the tensor component of the bare interaction on the isospin asymmetry of the optical potential [31]. In this work, we use Gogny D1S interaction which does not contain any tensor component. Gogny interaction can be considered as a parametrization of a g-matrix. Part of the bare tensor contribution is included in particular in the central term of Gogny interaction [37]. Moreover, elastic scattering calculations based on g-matrix have shown small differences with or without the g-matrix tensor component. Nonetheless, the addition of a tensor contribution in Gogny interaction has an effect both on the description of excited states with RPA [38] and on the coupling vertices in NSM. This effect of the tensor interaction has been investigated by Robin *et al.* [39] within a relativistic formalism. A consistent inclusion of a tensor contribution in Gogny interaction could help disentangle this issue. This is far beyond the scope of this work.

4 Volume integrals

Volume integrals are useful means of comparison between local potentials as they are well constrained by scattering data. When considering nonlocal potentials, volume integrals are well constrained only in a multipole range depending on incident energy. Nevertheless, they still provide interesting information. For instance, in a previous work [9] volume integral of the real part of NSM potential showed to be well suited for incident energies below about 30 MeV and too attractive for energies above this limit. Here we focus on the imaginary part of NSM potential which is nonlocal and energy dependent. When solving the integro-differential Schrödinger equation, it is convenient to use a multipole expansion of the nonlocal potential

$$V(\mathbf{r}\sigma, \mathbf{r}'\sigma'; E) = \sum_{ljm} \mathcal{Y}_{ljm}(\hat{\mathbf{r}}\sigma)\nu_{lj}(r, r'; E)\mathcal{Y}^{\dagger}_{ljm}(\hat{\mathbf{r}}'\sigma'), \quad (9)$$

where

$$\mathcal{Y}_{ljm}\left(\hat{\mathbf{r}}\sigma\right) \equiv \left[Y_l(\hat{\mathbf{r}}) \otimes \chi_{1/2}(\sigma)\right]_{jm}, \quad (10)$$

with $Y_l^{m_l}(\hat{r})$ the spherical harmonic and $\chi_{1/2}^{m_s}(\sigma)$ the spin function. In the case of a spherical target-nucleus, the potential is diagonal in (l, j), the multipole expansion of Schrödinger equation is decoupled and it can be solved independently at a given (l, j) with the corresponding $\nu_{lj}(r, r'; E)$ potential. The volume integral of the imaginary part of the nonlocal potential for a given multipole (l, j) is defined as

$$J_W^{lj}(E) = \frac{-4\pi}{A} \int \mathrm{d}r\, r^2 \int \mathrm{d}r' r'^2\, \mathrm{Im}[\nu_{lj}(r, r', E)], \quad (11)$$

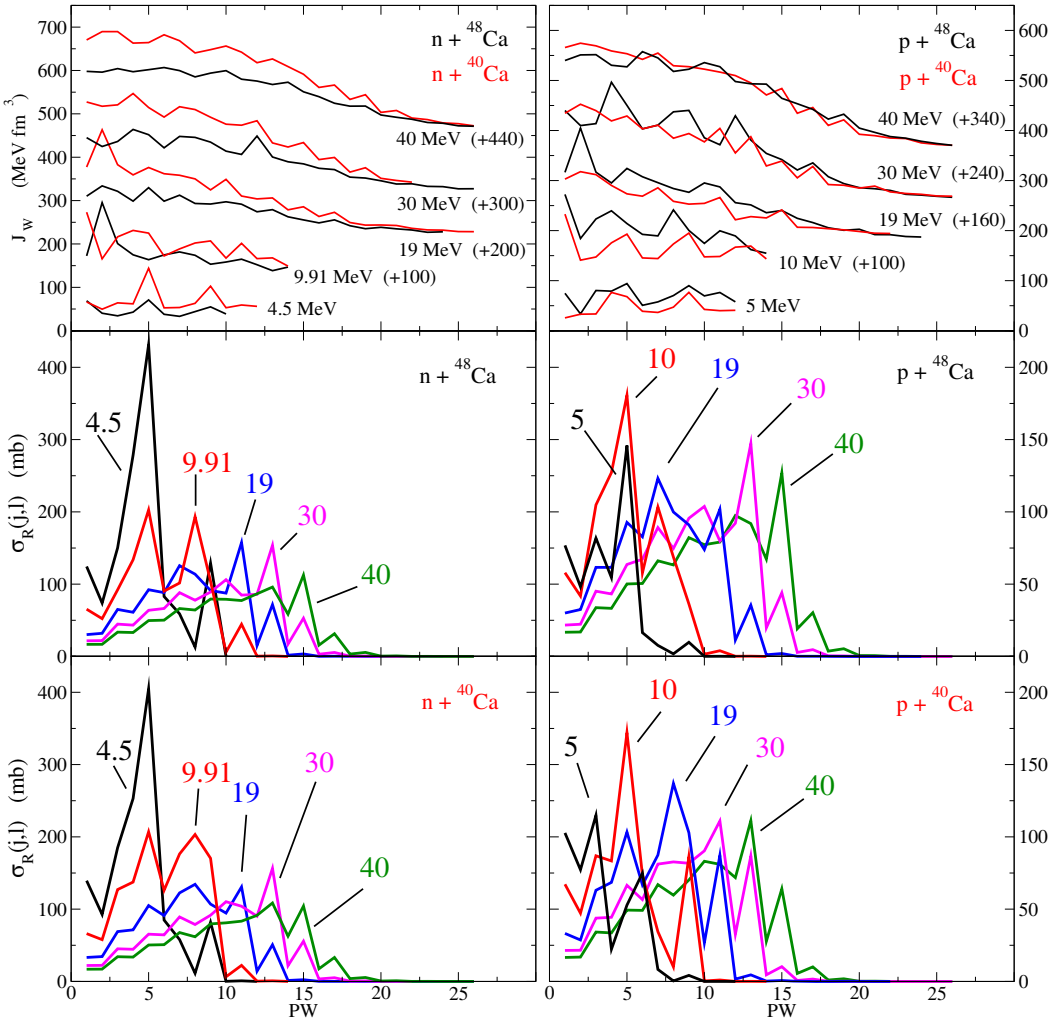

Fig. 5. (Color online) Volume integrals of the imaginary part of NSM potential for neutron and proton scattering off ^{40,48}Ca (top panels) as a function of partial waves. PW $= 1, 2, 3, \ldots$ stand for $(j, l) = (1/2, 0), (1/2, 1), (3/2, 1) \ldots$, partial waves, respectively. The lines have been offset along the y-axis by the indicated amounts. Reaction cross section as a function of multipole for the four reactions considered (four lower panels). Energies are indicated in MeV. Scales are different for each picture.

where A is the nucleon number of the target. In comparison, a local potential has volume integral which is independent of the multipole. Volume integrals of the imaginary part of NSM potential for neutron and proton scattering off ^{40,48}Ca are shown in the top panels of fig. 5. In the lower panel we present reaction cross sections for each multipole in order to emphasize multipoles contributing the most for each incident energy. At low incident energy the potential needs to be accurate for low multipoles as the Schrödinger equation is blind to what happens in higher multipoles. When the incident energy increases the potential needs an accuracy over higher multipole region. This partial-wave selectivity is the reason why an energy-dependent local potential, thus independent of the multipole, can be efficient in reproducing scattering observables. The only condition for a local potential to work is to be well tuned in the multipole region of interest for a given energy.

In the case of neutron scattering in fig. 5, we observe a reduction of the volume integral going from ^{40}Ca target to ^{48}Ca using NSM. This effect is observed for incident neutrons at all energies considered below 40 MeV. This is a clear indication of the asymmetry of the neutron NSM potential. The asymmetry of the neutron potential in calcium isotopes has been questioned by Charity *et al.* fitting dispersive potential [29]. This study has motivated new experiments and a new optical potential analysis by Mueller *et al.* [40]. They study the surface and the volume magnitudes of the potential and conclude that the neutron imaginary surface potential displays very little dependence on the neutron-proton asymmetry when going from ^{40}Ca target to ^{48}Ca one. Using radial integral rules for Woods-Saxon form factors, one shows that this behavior of the potential magnitude results in a depletion of about 6% of the volume integral, where NSM results for ^{40}Ca and ^{48}Ca approach each other. This is mainly due to the normalization by the total number of nucleons in eq. (11). The trend displayed in fig. 5 based on NSM is

the same to the one reported by Mueller *et al.*, although the asymmetry in the former appears more pronounced.

Below about 30 MeV incident energy, NSM potential for proton scattering provides the opposite trend than the one obtained with neutrons, featuring an enhancement of the volume integral going from ^{40}Ca target to ^{48}Ca. When the incident energy is increased, the asymmetry vanishes and volume integrals for the two calcium isotopes become comparable at ~ 40 MeV. Charity *et al.* deduced the same behavior for proton scattering doing an optical model analysis of elastic scattering data [29]. This means that for proton scattering, the NSM approach retains isospin asymmetry through couplings to excited states of the target. The further inclusion of the two-fold charge exchange component shown to be important in proton scattering off ^{48}Ca in sect. 3 would allow for coupling to Gamow-Teller modes and should increase both absorption and volume integrals.

5 Perey-Buck equivalent potential

Presently, NSM ability to reproduce elastic scattering observables is encouraging but not competitive enough from the point of view of evaluation standards. Nevertheless, NSM can provide some guidance for further nonlocal potential parametrizations. Moreover there is a renewal of interest in the community for nonlocal potentials and their impact on reaction calculations [41–45]. In this section, we present results of the fit of NSM imaginary potential using a Perey-Buck (PB)-like form factor [16]. The potential ansatz is built from a volume part and a surface part, each one with a different Gaussian nonlocality. Hopefully, the fitted potentials shall yield cross sections equivalent to the ones obtained with NSM. In practice, PB-like imaginary potential reads

$$\begin{aligned} &W^{n/p}(\mathbf{r},\mathbf{r}';E) = \\ &H(\mathbf{s},\beta_v)W_v^{n/p}(E-E_F^{n/p})f(R,r_v,a_v) \\ &+4a_sH(\mathbf{s},\beta_s)W_s^{n/p}(E-E_F^{n/p})f'(R,r_s,a_s), \end{aligned} \tag{12}$$

where we use notations $R=|\boldsymbol{r}+\boldsymbol{r}'|/2$ and $\mathbf{s}=\mathbf{r}-\mathbf{r}'$. v (s) subscript refers to parameters attributed to the volume (surface) part of the potential. $W_{v/s}^{n/p}(E-E_F^{n/p})$ is the energy-dependent magnitude of the potential, which varies for incident neutron and proton. $E_F^{n/p}$ represents the Fermi energy, while β corresponds to the nonlocality parameter. The volume term is built from a Woods-Saxon form factor,

$$f(r,r_0,a)=\left[1+\exp\left(\frac{r-r_0A^{1/3}}{a}\right)\right]^{-1}, \tag{13}$$

and surface term from a Woods-Saxon derivative with respect to r, $f'(r)$. r_0 and a are reduced radius and diffuseness, respectively. The nonlocal form factor reads

$$H(\mathbf{s},\beta)=\frac{1}{\pi^{3/2}\beta^3}\exp\left(-\left|\frac{\mathbf{s}}{\beta}\right|^2\right). \tag{14}$$

Table 1. PB-like parametrization of NSM for neutron and proton projectiles for ^{40,48}Ca targets. All parameters are expressed in fm.

r_v	r_s	a_v	a_s	β_v	β_s
0.78	1.254	0.49 (^{40}Ca) 0.78 (^{48}Ca)	0.44	0.35	1.1

We consider a Gaussian shape as in the original Perey-Buck phenomenological potential. Moreover this shape has already shown to provide a good description of NSM imaginary potential nonlocality [15]. It is worth mentioning that the Gaussian shape obtained with NSM is not related to the use of Gogny interaction which is itself built from Gaussian form factors. The same nonlocality shape is obtained using Skyrme interactions [19,46]. In the present work, two different nonlocality parameters are required in order to describe the surface and the volume contributions of the potential. Then following Perey *et al.* [16] prescription, the use of $|\mathbf{r}+\mathbf{r}'|\approx(r+r')$ allows for the multipole decomposition of the potential, as shown in eq. (9),

$$H_l(r,r',\beta)=\frac{4}{\sqrt{\pi}\beta^3}i^l j_l\left(-i\frac{2rr'}{\beta^2}\right)\exp\left(-\frac{r^2+r'^2}{\beta^2}\right), \tag{15}$$

where j_l is the spherical Bessel function. Finally the multipole expansion of the potential reads

$$\begin{aligned} &W_l^{n/p}(r,r';E) = \\ &H_l(r,r',\beta_v)W_v^{n/p}(E-E_F^{n/p})f(R,r_v,a_v) \\ &+4a_sH_l(r,r',\beta_s)W_s^{n/p}(E-E_F^{n/p})f'(R,r_s,a_s). \end{aligned} \tag{16}$$

The multipole expansion of the integro-differential Schrödinger equation can be found for example in ref. [15]. In a first attempt we do not consider any imaginary spin-orbit contribution. As a consequence the multipole expansion is only l-dependent. Fitted parameters obtained for incident energies below 40 MeV are gathered in table 1. Except for the diffuseness of the volume component, a single parameter set is obtained for both ^{40}Ca and ^{48}Ca. We find a different reduced radius for the surface and the volume contribution. Surface reduced radius, r_s, is close to the value generally adopted in optical potential analyses. Volume reduced radius, r_v, is quite small. This small value of the volume radius is somehow compensated by a deeper volume magnitude. Regarding nonlocalities, the NSM approach predicts a smaller nonlocality parameter for the volume part of the potential than for the surface one. Mahzoon *et al.* have found the same trend in their optical model analysis with a nonlocal potential [41].

Despite the fact that PB-like potential is a rather simple ansatz to represent NSM potential, it provides a rough idea of the shape of the potential. In fig. 6 we present a sample of the fit for proton scattering off ^{48}Ca at 30 MeV. For imaginary potential we adopt positive values when absorptive. For sake of concision we only present the first four multipoles of the potential but a reasonable agreement is obtained as well for higher multipoles. Diagonal ($r=r'$) contributions are fitted using the ansatz of eq. (16). They

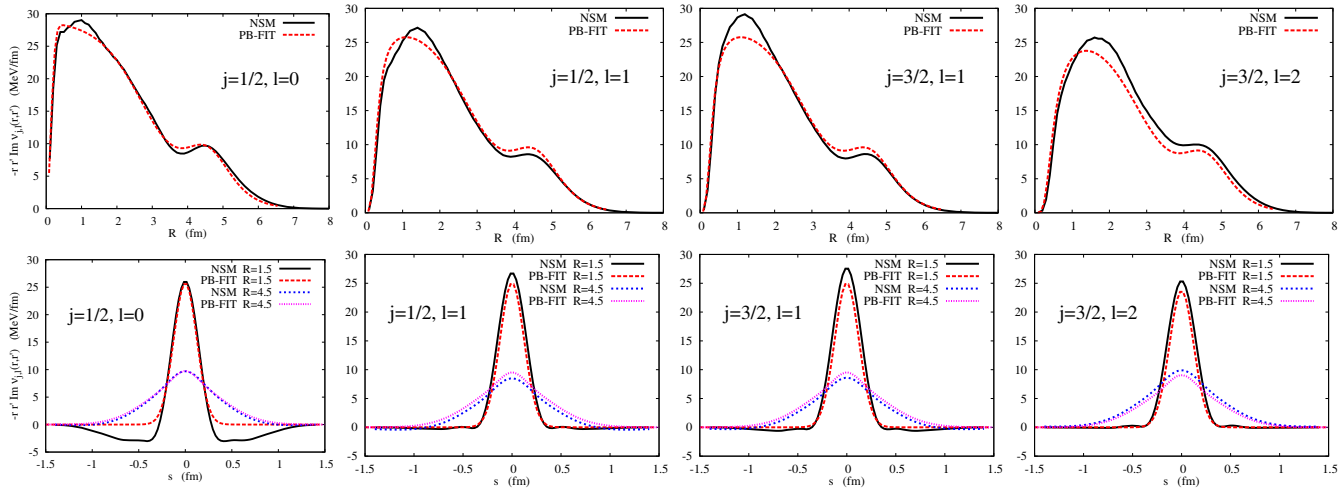

Fig. 6. Sample of PB-like potential fit of NSM for the first four multipoles for proton scattering off ^{48}Ca at 30 MeV (top panels). Diagonal contribution of the potential multipole expansion: NSM and fit (bottom panels), with corresponding nonlocal contribution at $R = 1.5$ fm and $R = 4.5$ fm.

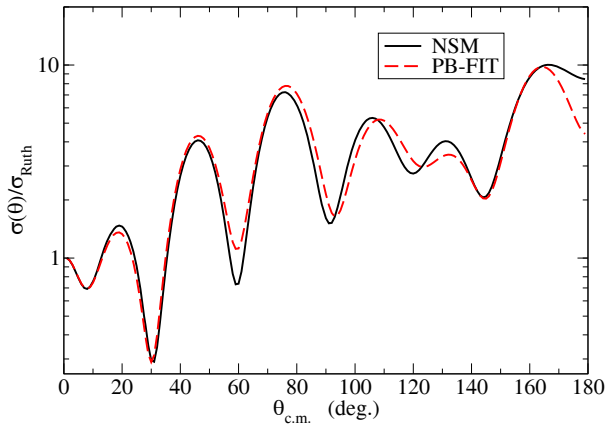

Fig. 7. Comparison between differential elastic cross sections for proton scattering off ^{48}Ca at 30 MeV obtained with NSM and with the equivalent PB-like potential.

are presented in the top panels of fig. 6. The surface and the volume nonlocality parameters are adjusted as well by looking at two transversal cuts of the nonlocal potential at $R = 1.5$ fm and $R = 4.5$ fm, respectively. Corresponding results are presented in the lower panels of fig. 6. In the first multipole emissive "wings" appear in the nonlocality at various incident energies. We do not take this effect into account in order to keep the form factor used for the fit as simple as possible. Moreover, the first multipole is expected to play a major role mainly at very low scattering energy.

Then we check the ability of the PB-like potential to describe differential elastic cross section obtained with NSM. As shown in fig. 7 in the case of proton scattering off ^{48}Ca at 30 MeV, agreement is good enough to consider that the fit retains the main features of NSM potential. The same agreement is obtained for all the cases discussed. Then one can explore the behavior of the magnitudes for the surface and the volume contributions as a function of energy and projectile and look for evidences of asymmetry. Results of the fit of the magnitudes for neutron and proton scattering for ^{40,48}Ca are summarized in fig. 8. Magnitudes are depicted as a function of incident energy subtracted by Fermi energy given in table 2. For simplicity we use Fermi energies obtained from HF calculations which corresponds to the energy of the last fully occupied orbital. In reality one should determine the Fermi energy taking into account the energy dependent RPA contribution to the real part but at this stage our implementations is not yet suited in order to describe negative energies. Nevertheless, this contribution is expected to be small.

Results for ^{40}Ca (fig. 8, top panel) show that neutron and proton magnitudes both follow the same trend for surface and volume components. This is what is expected from a Lane consistent potential for scattering off self-conjugate target nucleus [17]. The same behavior has been observed by Mueller *et al.* [40] without imposing Lane consistency during the fit procedure.

Going from ^{40}Ca to ^{48}Ca the proton surface magnitude is increased whereas the neutron one follows the opposite trend. In the meantime, volume magnitudes for both neutron and proton are reduced of about 10 MeV. Once again this is a proof of asymmetry already retained at the level of the coupling to excited states of the target. As we have seen in sect. 3, NSM leads to a lack of absorption in the description of proton scattering off ^{48}Ca. By comparison with TALYS, this has been attributed to the absence of two-fold charge exchange (p, n, p) contribution avoiding coupling to Gamow-Teller mode, so we can expect asymmetry in the proton case to be enhanced when including two-fold charge exchange. Considering neutron magnitudes the observed asymmetry with NSM is in disagreement with results obtained by Mueller *et al.* [40] who predicted no asymmetry going from ^{40}Ca to ^{48}Ca for neutron scattering.

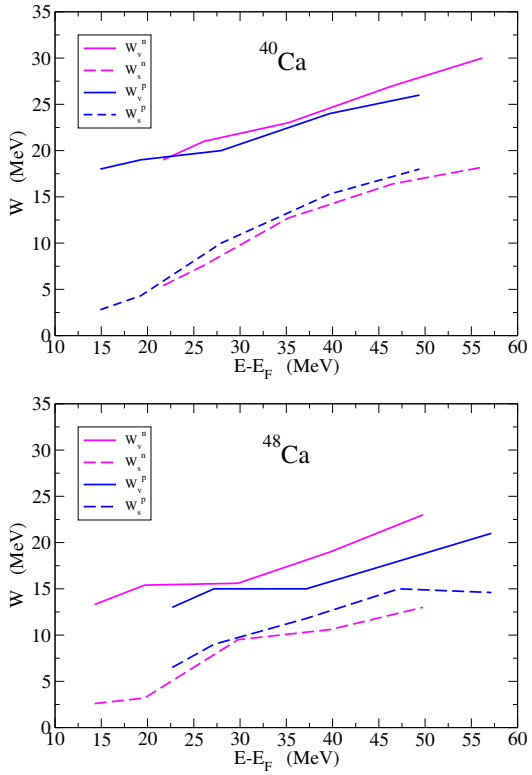

Fig. 8. Magnitude of surface and volume parts of Perey-Buck-like potential fitted from NSM for neutron and proton scattering off ^{40,48}Ca.

In the Lane model [17], which assumes isospin symmetry in nuclei, the nucleon-nucleus potential can be decomposed into isoscalar V_0 and isovector V_1 parts,

$$V^{(n/p)} = V_0 \pm \frac{(N-Z)}{2A} V_1, \qquad (17)$$

where (+) stands for neutron projectile and (−) for proton projectile. N (P) is the neutron (proton) number in the target nucleus. As already discussed by Osterfeld *et al.* [47], NSM contains by construction Lane inconsistent terms. Indeed the difference between neutron potential and proton potential,

$$V^n - V^p = \frac{N-Z}{A} V_1 - V_{cc}, \qquad (18)$$

can be due not only to the isospin conserving Lane potential as stated in eq. (17) but also to isospin nonconserving Coulomb corrections, V_{cc}. These Coulomb corrections stem from the second-order part of the potential. Both theoretical [48] and empirical [49] findings indicate that Coulomb correction weakens the absorption for protons compared to that for neutrons at the same energy. Nevertheless, Osterfeld *et al.* have shown that Coulomb correction in the case of ^{40}Ca [47] is small, what is confirmed by our results on magnitude in fig. 8. Hence one can safely consider eq. (17) as a reasonable approximation for ^{40}Ca in the considered energy range. On the opposite, Coulomb correction is not negligible in the case of ^{48}Ca [50]. Neglecting Coulomb correction in eq. (18), one can in principle recover an upper limit of the absorption for proton scattering off ^{48}Ca.

Table 2. HF Fermi energies in MeV.

E_F^n $(A=40)$	E_F^p $(A=40)$	E_F^n $(A=48)$	E_F^p $(A=48)$
−16.19	−9.39	−9.77	−17.17

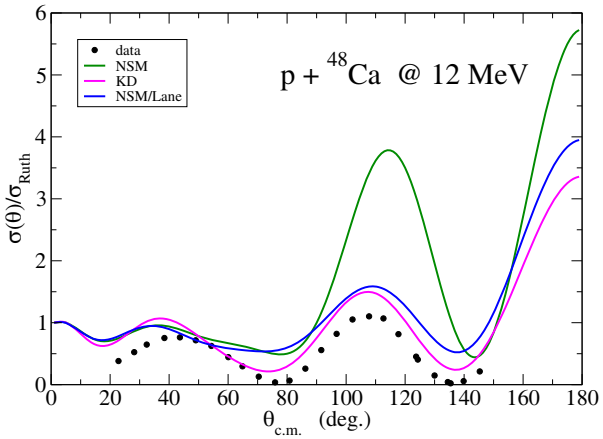

Fig. 9. Differential elastic cross sections obtained with NSM (green curve), Koning-Delaroche global potential (magenta curve) and NSM with Lane correction (blue curve) compared with data for proton scattering off ^{48}Ca at 12 MeV.

In the case of nucleon scattering off ^{40}Ca ($N = Z = 20$), Lane model leads to the same potential for neutron and proton projectile. One can parametrize the ^{40}Ca potential using the ansatz of eq. (16). Then using the same parametrization with $A = 48$, one gets the isoscalar part of the potential V_0^{FIT} extrapolated for ^{48}Ca. Assuming NSM reasonably describes neutron scattering off ^{48}Ca as shown in sect. 3, one finally gets an NSM/Lane version of the proton-^{48}Ca potential,

$$V^p_{NSM/Lane}(^{48}\mathrm{Ca}) = 2V_0^{FIT}(^{48}\mathrm{Ca}) - V^n_{NSM}(^{48}\mathrm{Ca}), \qquad (19)$$

where NSM potential is used for the neutron-^{48}Ca potential. As a first test case in fig. 9, we present the differential elastic cross section for proton scattering off ^{48}Ca at 20 MeV. NSM/Lane prescription is used for the imaginary part of the potential whereas the real part is kept as the one used in NSM calculations presented in sect. 3. The use of NSM/Lane potential described in eq. (19) greatly improves the description of the cross section by substantially enhancing the absorption. Cross sections presented in linear scale are very close to that from the Koning-Delaroche benchmark.

Higher-order versions of Lane prescription have been investigated by Holt *et al.* [12] and could be relevant in the ^{48}Ca case. Nevertheless, one has to keep in mind that formally NSM potential contains Lane-inconsistent terms in the second order terms. So one should be careful in taking into account the two-fold charge exchange in order to get a fully reliable description of the potential.

6 Conclusions

A study of neutron and proton scattering off ^{40}Ca and ^{48}Ca targets has been undertaken using the Nuclear Structure Method for scattering. Gogny D1S nucleon-nucleon effective interaction is used consistently throughout the determination of the optical potential. NSM provides a reasonable description of neutron scattering off ^{40,48}Ca and proton scattering off ^{40}Ca below about 30 MeV incident energy. On the other hand, a default of absorption is observed in differential cross sections for proton scattering off ^{48}Ca for all considered incident energies between 8 MeV and 30 MeV. An independent calculation using TALYS evaluation tool has evidenced the importance of direct neutron emission in that case. This result points out the importance of two-fold charge exchange in proton scattering off ^{48}Ca. This is most probably the case in general for proton scattering off neutron-rich targets inclined to emit neutrons.

The study of multipole dependent volume integrals of nonlocal NSM imaginary contribution reveals that NSM predicts asymmetry for neutron scattering going from ^{40}Ca target to the ^{48}Ca one. Above ~ 30 MeV, the asymmetry tends to diminish leading to comparable contributions at about 40 MeV. Results obtained for proton scattering should be modified when accounting for (p, n, p) two-fold charge exchange.

Then we have proceeded to a fit of the NSM imaginary potential with a Perey-Buck-like potential extracting in particular magnitudes for neutron and proton projectiles and for ^{40}Ca and ^{48}Ca targets. Results for neutron and proton potentials for scattering off ^{40}Ca indicate that Lane-inconsistent terms in the NSM potential are small in that case. Based on this observation, we have used Lane prescription to account for the lack of absorption observed in proton scattering off ^{48}Ca, obtaining a significant improvement. Nevertheless, the NSM potential contains Lane-inconsistent terms by construction and the issue of two-fold charge exchange will have to be faced in further attempts following, for example, the work by Osterfeld *et al.* [47].

Study of heavier double-closed-shell targets is in progress. Moreover the extension to target nuclei experiencing pairing using Gorkov formalism has been initiated for spherical targets. This will open access to hundred of new targets.

HFA wishes to thank the colleagues of CEA, DAM, DIF for their kind hospitality during his stay at Bruyères-le-Châtel, where part of his contribution to this collaboration took place.

References

1. G. Satchler, *Direct Nuclear Reactions*, in *International Series of Monographs on Physics* (Clarendon Press, 1983).
2. W. Hauser, H. Feshbach, Phys. Rev. **87**, 366 (1952).
3. P.A. Moldauer, Phys. Rev. **123**, 968 (1961).
4. C.A. Engelbrecht, H.A. Weidenmüller, Phys. Rev. C **8**, 859 (1973).
5. D. Bès, R. Broglia, G. Dussel, R. Liotta, R. Perazzo, Nucl. Phys. A **260**, 77 (1976).
6. G. Potel, A. Idini, F. Barranco, E. Vigezzi, R.A. Broglia, Rep. Prog. Phys. **76**, 106301 (2013).
7. N. Vinh Mau, *Theory of Nuclear Structure* (IAEA, Vienna, 1970) p. 931.
8. K. Mizuyama, K. Ogata, Phys. Rev. C **86**, 041603 (2012).
9. G. Blanchon, M. Dupuis, H.F. Arellano, N. Vinh Mau, Phys. Rev. C **91**, 014612 (2015).
10. T.V. Nhan Hao, B.M. Loc, N.H. Phuc, Phys. Rev. C **92**, 014605 (2015).
11. G. Hagen, N. Michel, Phys. Rev. C **86**, 021602 (2012).
12. J.W. Holt, N. Kaiser, G.A. Miller, Phys. Rev. C **93**, 064603 (2016).
13. M. Dupuis, S. Karataglidis, E. Bauge, J.P. Delaroche, D. Gogny, Phys. Rev. C **73**, 014605 (2006).
14. H.F. Arellano, E. Bauge, Phys. Rev. C **84**, 034606 (2011).
15. G. Blanchon, M. Dupuis, H.F. Arellano, Eur. Phys. J. A **51**, 165 (2015).
16. F. Perey, B. Buck, Nucl. Phys. **32**, 353 (1962).
17. A. Lane, Nucl. Phys. **35**, 676 (1962).
18. P. Ring, P. Schuck, *The Nuclear Many-Body Problem* (Springer, 2004).
19. V. Bernard, N. Van Giai, Nucl. Phys. A **327**, 397 (1979).
20. J.F. Berger, M. Girod, D. Gogny, Comput. Phys. Commun. **63**, 365 (1991).
21. J. Raynal, computer code DWBA98, 1998 (NEA 1209/05).
22. C. Rao, M. Reeves III, G. Satchler, Nucl. Phys. A **207**, 182 (1973).
23. J. Blaizot, D. Gogny, Nucl. Phys. A **284**, 429 (1977).
24. V. De Donno, G. Co', M. Anguiano, A.M. Lallena, Phys. Rev. C **83**, 044324 (2011).
25. A.J. Koning, J.P. Delaroche, Nucl. Phys. A **713**, 231 (2003).
26. A.J. Koning, S. Hilaire, M. Duijvestijn, in *Proceeding of the International Conference on Nuclear Data for Science and Technology-ND2007* (EDP Sciences, Paris, France, 2008) pp. 211–214.
27. Y. Xu, H. Guo, Y. Han, Q. Shen, J. Phys. G: Nucl. Part. Phys. **41**, 015101 (2014).
28. R.J. Charity, L.G. Sobotka, W.H. Dickhoff, Phys. Rev. Lett. **97**, 162503 (2006).
29. R.J. Charity, J.M. Mueller, L.G. Sobotka, W.H. Dickhoff, Phys. Rev. C **76**, 044314 (2007).
30. R.J. Charity, W.H. Dickhoff, L.G. Sobotka, S.J. Waldecker, Eur. Phys. J. A **50**, 1 (2014).
31. S.J. Waldecker, C. Barbieri, W.H. Dickhoff, Phys. Rev. C **84**, 034616 (2011).
32. C. Barbieri, W.H. Dickhoff, Phys. Rev. C **63**, 034313 (2001).
33. D. Gambacurta, M. Grasso, F. Catara, Phys. Rev. C **81**, 054312 (2010).
34. N. Pillet, N. Sandulescu, P. Schuck, Phys. Rev. C **76**, 024310 (2007).
35. J. Raynal, computer code ECIS03, 2004 (NEA 0850/16).
36. A. Koning, M. Duijvestijn, Nucl. Phys. A **744**, 15 (2004).
37. R.N. Bernard, M. Anguiano, Nucl. Phys. A **953**, 32 (2016).
38. M. Anguiano, A.M. Lallena, G. Co', V. De Donno, M. Grasso, R.N. Bernard, Eur. Phys. J. A **52**, 183 (2016).
39. C. Robin, E. Litvinova, Eur. Phys. J. A **52**, 205 (2016).
40. J.M. Mueller, R.J. Charity, R. Shane, L.G. Sobotka, S.J. Waldecker, W.H. Dickhoff, A.S. Crowell, J.H. Esterline, B. Fallin, C.R. Howell *et al.*, Phys. Rev. C **83**, 064605 (2011).

41. M.H. Mahzoon, R.J. Charity, W.H. Dickhoff, H. Dussan, S.J. Waldecker, Phys. Rev. Lett. **112**, 162503 (2014).
42. L.J. Titus, F.M. Nunes, Phys. Rev. C **89**, 034609 (2014).
43. A. Ross, L.J. Titus, F.M. Nunes, M.H. Mahzoon, W.H. Dickhoff, R.J. Charity, Phys. Rev. C **92**, 044607 (2015).
44. L.J. Titus, F.M. Nunes, G. Potel, Phys. Rev. C **93**, 014604 (2016).
45. A. Ross, L.J. Titus, F.M. Nunes, Phys. Rev. C **94**, 014607 (2016).
46. A. Bouyssy, H. Ngô, N. Vinh Mau, Nucl. Phys. A **371**, 173 (1981).
47. F. Osterfeld, V.A. Madsen, Phys. Rev. C **24**, 2468 (1981).
48. J.P. Jeukenne, A. Lejeune, C. Mahaux, Phys. Rev. C **16**, 80 (1977).
49. J. Rapaport, Phys. Lett. B **92**, 233 (1980).
50. F. Osterfeld, V.A. Madsen, Phys. Rev. C **32**, 108 (1985).